Journal of
Materials Chemistry C

ROYAL SOCIETY
OF CHEMISTRY

REVIEW

View Article Online
View Journal

Cite this: DOI: 10.1039/d5tc03998c

Atomic force microscopy for ferroelectric materials research

Yeongyu Kim,†[a] Kunwoo Park,†[a] Seonggon Han,[a] Dongyan Chen,[a] Donghun Kim,[a] Gumin Kang[a] and Seungbum Hong*[ab]

The behavior of ferroelectric materials is governed by phenomena such as polar surface screening, domain nucleation and growth, and interaction between polarization and defects at the nanoscale. However, traditional macroscopic characterization methods lack spatial resolution to resolve these local phenomena. Atomic force microscopy (AFM) has uniquely filled this gap, evolving from a simple imaging tool into an indispensable platform for both probing and actively manipulating the polarization domain and domain wall. This review encompasses the significant advancements in multimodal AFM, demonstrating how its ability to locally characterize and manipulate them provides fundamental insights. Furthermore, we emphasize the critical role of AFM in validating ferroelectricity in emergent materials, where macroscopic techniques are facing critical challenges. This study provides a comprehensive framework, linking the fundamental physics of nanoscale domains and interfaces to the intrinsic functionality of ferroelectric materials.

Received 10th November 2025,
Accepted 12th January 2026

DOI: 10.1039/d5tc03998c

rsc.li/materials-c

1. Introduction

Ferroelectric materials exhibiting spontaneous electric polarization that can be reversibly switched by an external electric field, have been a central focus of condensed matter physics and materials science for several decades.[1–7] The inherently switchable polarization is the origin of their rich portfolio of functional properties, such as piezoelectricity, pyroelectricity, and non-linear optical effects, making them a fascinating class of materials for versatile application fields.[8–14] Historically, the understanding of these properties was primarily based on macroscopic, bulk scale measurements.[1,11,15] While the classical viewpoint has been foundational to ferroelectric materials research, it often does not fully interpret the intricate local phenomena at the nanoscale. This challenge arises because macroscopic characterization methods inherently average the local polar response of the materials.[15] In particular, the bulk-averaging approach might induce ambiguous interpretation for

Yeongyu Kim

Yeongyu Kim is a PhD candidate in the Department of Materials Science and Engineering at KAIST. He received his MS and BS degrees in the School of Materials Science and Engineering at Kyungpook National University (KNU). His research interests include probing the local electrical and structural properties in ferroelectrics and 2D materials using advanced AFM techniques.

Kunwoo Park

Kunwoo Park is a PhD candidate in the Department of Materials Science and Engineering at KAIST. He received his BS degree in the Division of Materials Science and Engineering at Hanyang University. His research interests include ferroelectrics and advanced 3D imaging techniques via AFM tomography.

---

[a] Department of Materials Science and Engineering, Korea Advanced Institute of Science and Technology (KAIST), Daejeon, 34141, Republic of Korea. E-mail: seungbum@kaist.ac.kr

[b] KAIST Institute for NanoCentury (KINC), KAIST, Daejeon, 34141, Republic of Korea

† These authors contributed equally to this work.

the precise mechanisms of domain nucleation, the complex interactions between domain walls and defects, and the non-trivial intricacies of surface charge screening.[8,13,14,16]

It is now widely recognized that the local contributions are not minor perturbations; rather, the nanoscale phenomena are the very foundation of the macroscopic properties and ultimately govern the macroscopic response of ferroelectric materials.[17–20] Consequently, developing a deeper understanding of the origins of ferroelectricity demands the need for a technique capable of probing local electromechanical and electrostatic properties directly at their relevant length scales.[21,22] In this regard, atomic force microscopy (AFM) has emerged as the essential tool for this purpose.[23–30] By utilizing its advanced functional modes, AFM can locally map the key signatures of ferroelectricity – such as the nanoscale configuration of polarization domains, the local surface charge distribution, the domain wall conductivity – providing direct, spatially resolved insights into the fundamental physics underpinning the local polarization behavior.[27,31–33]

This review focuses on AFM-based approaches as the key enabling tools for probing the nanoscale behavior of ferroelectric materials, emphasizing their seminal contributions to the field. We first provide a brief overview of the fundamental properties of ferroelectric materials that are central to these advanced nanoscale measurements. Then, the primary AFM methodologies employed for both local characterization and nanoscale manipulation are reviewed. The core of this review explores how the unique capabilities of AFM are applied to investigate complex domain physics, polarization switching dynamics, and local surface charge phenomena. We also discuss the role of AFM as a platform for nanoscale engineering of intentionally structuring domain patterns *via* local tip-induced stimuli, which creates model systems for fundamental study. By systematically examining these topics, we provide a framework for understanding how AFM has profoundly advanced our fundamental knowledge of nanoscale local polar behaviors in ferroelectrics. This study offers a comprehensive basis for researchers aiming to further understand and control these complex nanoscale behaviors.

Seungbum Hong

Seungbum Hong received his BS, MS, and PhD degrees from KAIST. He served as a project manager and team leader at the Samsung Advanced Institute of Technology (SAIT), and subsequently as a tenured staff scientist at Argonne National Laboratory. In 2017, he returned to KAIST as a professor in the Department of Materials Science and Engineering and currently serves as the Vice President of Academic Affairs. His research group investigates the physics of ferroelectric and piezoelectric domains, electrochemical phenomena in battery materials, and the integration of artificial intelligence into materials research.

2. Fundamentals of ferroelectric materials

Ferroelectric materials are defined as polar crystals that exhibit spontaneous polarization (P_S) with at least two stable equilibrium orientations in the absence of an external electric field, which can be reoriented between these distinct states by an applied field.[34,35] The ferroelectricity is rooted in crystallographic asymmetry, which places ferroelectric materials within a nested hierarchy: they are a specialized subset of pyroelectric materials, which are themselves a subset of piezoelectric materials. Pyroelectric materials, the parent class, are also characterized by a spontaneous polarization; however, it is non-switchable and its magnitude is temperature-dependent.[10] Piezoelectric materials, the broadest of these classes, are defined by the linear coupling between an applied mechanical stress and the resulting electric polarization.[11]

The P_S of a ferroelectric material vanishes above a critical temperature known as the Curie temperature (T_C), at which the material undergoes a structural phase transition into a non-polar paraelectric state. The phase transition is phenomenologically described by the Landau–Ginzburg–Devonshire (LGD) theory, a framework that models the stability of polarization states by expanding the Gibbs free energy as a polynomial series with polarization as the order parameter.[36,37] According to the LGD theory, the free energy landscape above T_C is characterized by a single-well potential with its minimum at zero polarization, corresponding to the stable paraelectric phase (Fig. 1a). As the material is cooled below T_C, the energy landscape transforms into a characteristic double-well potential. In the ferroelectric state, the free energy is minimized at two distinct, non-zero polarization values of $\pm P_S$. The energy barrier separating these two stable states is what must be overcome to reorient the polarization, which is typically achieved by applying an external electric field, thus enabling the polarization switching fundamental to ferroelectricity.

While LGD theory describes the homogeneous energetic landscape for the phase transition, the actual polarization switching process is spatially inhomogeneous, proceeding *via* the nucleation and growth of ferroelectric domains.[17,38,39] The formation of the polar domain structure is a fundamental mechanism for the system to minimize its total free energy. In a hypothetical single-domain state, the P_S terminates at the surfaces of the material, resulting in a layer of uncompensated bound charges (Fig. 1b). These charges generate a significant internal electric field, known as the depolarization field, which opposes the P_S and renders the single-domain state energetically unstable.[40] To mitigate this prohibitive electrostatic energy, the crystal spontaneously divides into multiple domains – regions within which the polarization is uniformly

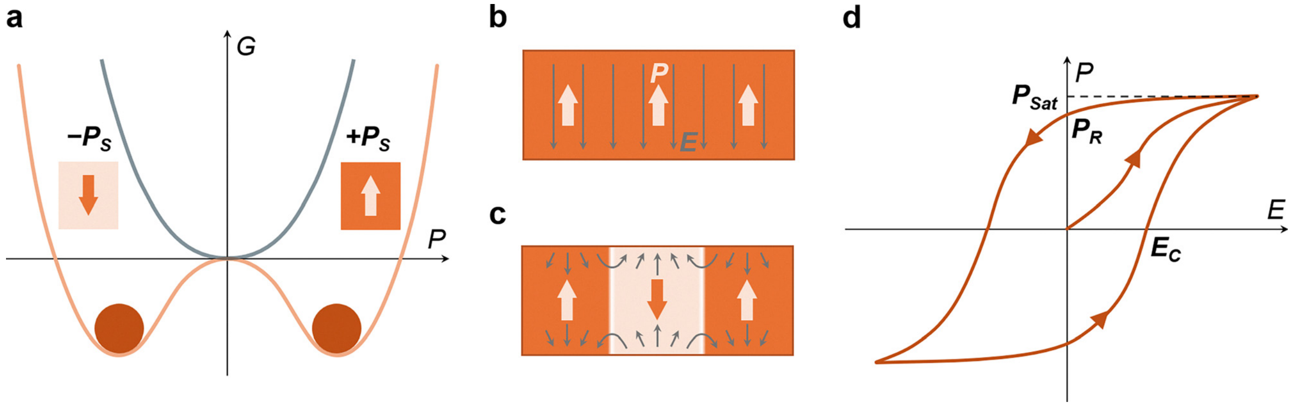

Fig. 1 Schematic illustrations of the fundamental properties of ferroelectric materials. (a) The LGD free energy potential. Above the T_C, the material is in a paraelectric state, characterized by a single-well potential (gray). Below T_C, it transitions to the ferroelectric state, described by a double-well potential with two stable $\pm P_S$ (orange). (b) Illustration of an energetically unfavorable single-domain state. The termination of polarization at the surfaces creates uncompensated bound charges, which generate a strong internal depolarization field. (c) Formation of a 180° multi-domain structure, which minimizes the prohibitive electrostatic energy of the single-domain state. This creates regions of uniform, opposing domains separated by domain walls. (d) The characteristic P–E hysteresis loop, a macroscopic consequence of domain-based switching. The P_{Sat}, P_R, and the E_C, are indicated.

oriented, but in different directions (Fig. 1c).[17,19] The narrow, transitional boundary separating two adjacent domains is known as a domain wall.

A direct consequence of the switching based on domain nucleation and growth is the characteristic ferroelectric hysteresis loop, a nonlinear relationship between the applied electric field (E) and the measured polarization (P) (Fig. 1d). At small E, the P increases linearly, as the energy is not yet strong enough to switch domains with unfavorable orientations. As the field strength increases, the domains begin to switch, leading to a rapid, nonlinear increase in P. Eventually, once all switchable domains are aligned with E, the material reaches a state of saturation polarization (P_{Sat}). Upon decreasing E from P_{Sat}, a significant P remains even when the field reaches zero; this value is the remnant polarization (P_R). To achieve a zero-polarization state, an opposite field must be applied, the magnitude of which is known as the coercive field (E_C). Further increasing the field in the negative direction saturates the polarization in the opposite orientation, completing the hysteresis cycle.

These key physical phenomena that govern ferroelectric behavior – domain structures, wall dynamics, and charge screening – are all inherently rooted in the nanoscale.[3,8] Consequently, conventional macroscopic measurements, which average over these crucial details, obscure the local mechanisms that define the ferroelectric properties. Probing these effects directly thus necessitates characterization techniques with high spatial resolution. AFM-based methods are uniquely suited for this challenge, serving not only as a passive characterization tool but also as a platform for active nanoscale manipulation. The AFM tip can apply localized electric or mechanical forces to precisely engineer domain structures to uncover novel physical phenomena. The multiple capability has made AFM an indispensable tool for advancing the fundamental understanding of ferroelectricity, as will be detailed in the following sections.

3. Multimodal AFM characterization of ferroelectric materials

To investigate the multifaceted nature of ferroelectric materials at the nanoscale, three principal AFM modalities are generally employed: piezoresponse force microscopy (PFM), Kelvin probe force microscopy (KPFM), and conductive AFM (C-AFM).[27,41,42] The primary technique for imaging the polarization domains themselves is PFM (Fig. 2a).[33,43] PFM operates by applying an AC voltage to a conductive tip in contact with the sample, inducing a local mechanical oscillation *via* the inverse piezoelectric effect. The resulting PFM amplitude correlates with the magnitude of the local piezoelectric coefficient, while the phase of the vibration relative to the applied AC voltage reveals the orientation of the polarization direction. The PFM phase signal, typically exhibiting a 180° contrast between anti-parallel domains, enables the direct visualization and mapping of domain configurations.[29] However, conventional single-frequency PFM often suffers from low signal or crosstalk if the resonance frequency of the cantilever shifts due to local mechanical variations. To address the challenge of maintaining resonance, dual-frequency resonance-tracking (DART) PFM is introduced.[44] Using an amplitude-based feedback loop with two excitation frequencies near its resonance peak, DART PFM continuously tracks the contact resonance in real time. This approach effectively decouples the desired piezoelectric signal from topographic or mechanical artifacts and dramatically improves the signal-to-noise ratio.[45,46]

To probe the associated electrostatic environment, KPFM is employed (Fig. 2b).[47] KPFM is a non-contact method to map the surface potential of the sample. It operates by applying a DC bias to the tip to nullify the electrostatic force arising from the Contact Potential Difference (CPD) between the tip and sample. The measured CPD is directly related to the local surface potential and is highly sensitive to polarization and surface charge. This provides spatially resolved insights into phenomena

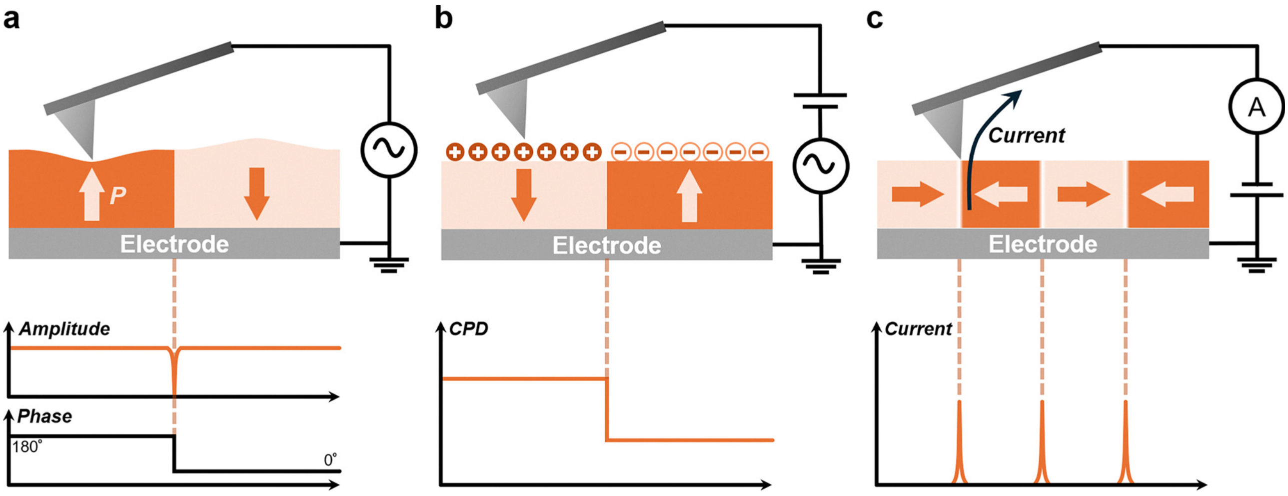

Fig. 2 Schematic illustrations of the primary AFM modalities for ferroelectric characterization. (a) The operating principle of PFM, where an AC voltage applied to a conductive tip induces a local mechanical oscillation *via* the inverse piezoelectric effect, which is measured as the PFM signal. When the applied voltage wave is compared to the mechanical response, a 180° phase shift is observed between domains with anti-parallel polarization orientations. (b) The operating principle of KPFM, which maps the surface potential by applying a DC bias to nullify the electrostatic force arising from the CPD between the tip and sample. (c) The operating principle of C-AFM, where a DC bias is applied to the sample in contact with the tip, and the resulting local current is measured to map electronic transport properties.

such as surface screening dynamics, domain-dependent work function, and the local depolarization fields.[31,48] Finally, C-AFM directly characterizes the local electronic transport properties (Fig. 2c).[49] By scanning a biased tip in direct contact with the sample surface, C-AFM visualizes maps of nanoscale current flow. C-AFM is essential for investigating polarization-modulated conductivity, identifying local leakage pathways, studying charge injection phenomena, and probing the anomalous conductive nature of domain walls.[50,51]

Within the PFM modality, two primary configurations are used to resolve the different components of the polarization vector and obtain comprehensive spatial domain information: vertical PFM (VPFM) and lateral PFM (LPFM).[52,53] VPFM is designed to detect the out-of-plane polarization component (P_z). It measures the vertical displacement of the sample surface (Fig. 3a), which results from the coupling between the applied vertical electric field (E_z) from the tip and the longitudinal piezoelectric coefficient (d_{33}^{eff}).[54] This allows for the mapping of domains polarized perpendicular to the sample surface (*i.e.*, up and down domains), where a 180° phase contrast typically distinguishes between these opposite orientations. Conversely, LPFM is sensitive to the in-plane polarization components (P_x, P_y). It measures the torsional twisting of the cantilever (Fig. 3b), which arises from the local shear deformation of the sample surface.[54,55] The shear strain is primarily attributed to the in-plane components of the electric field coupling with the shear piezoelectric coefficients (d_{15}^{eff}). LPFM is thus essential for visualizing domains polarized parallel to the sample plane. By acquiring both VPFM and LPFM signals simultaneously, a technique often referred to as vector PFM, it is possible to reconstruct the local polarization vector field with high spatial resolution.[56,57] The vector-resolved PFM approach is crucial for understanding complex domain configurations, including the precise orientation of domain walls, and is indispensable for mapping the intricate spatial distribution of polarization component found in emergent topological structures such as ferroelectric vortices and skyrmions-like domains (Fig. 3c).[58,59]

Beyond 2D surface mapping, PFM can be extended to volumetric visualization through tomographic approaches. This method, known as tomographic PFM (TPFM), involves the sequential, layer-by-layer removal of material, typically accomplished by scanning the AFM tip under a high applied load (Fig. 3d).[60] Following the removal of each thin layer, a standard PFM image is acquired at the newly exposed surface. By digitally stacking the series of 2D cross-sectional images and registering them to their known depths, a 3D reconstruction of the domain morphology within the excavated volume is generated. This technique overcomes the significant limitations of surface-only approaches, providing direct experimental insight into the complex internal domain architecture, the 3D tilting of domain walls, and the depth evolution of ferroelectric domains.[61,62]

While PFM probes the electromechanical strain response to reveal the amplitude and phase of the polarization vector, KPFM complements this by mapping the surface electrostatics. It measures the CPD to provide a quantitative understanding of the surface charge screening state.[31,48] This allows for the interpretation of how the bound polarization charges at the surface are compensated, whether by internal mobile electronic carriers or by external polar/ionic adsorbates.[63,64] A key observation on the surface of many ferroelectric materials is that the measured domain-dependent potential is often inverted in sign relative to the potential one would expect from the bound polarization charge alone. This phenomenon is typically attributed to complete or even over-screening by an external

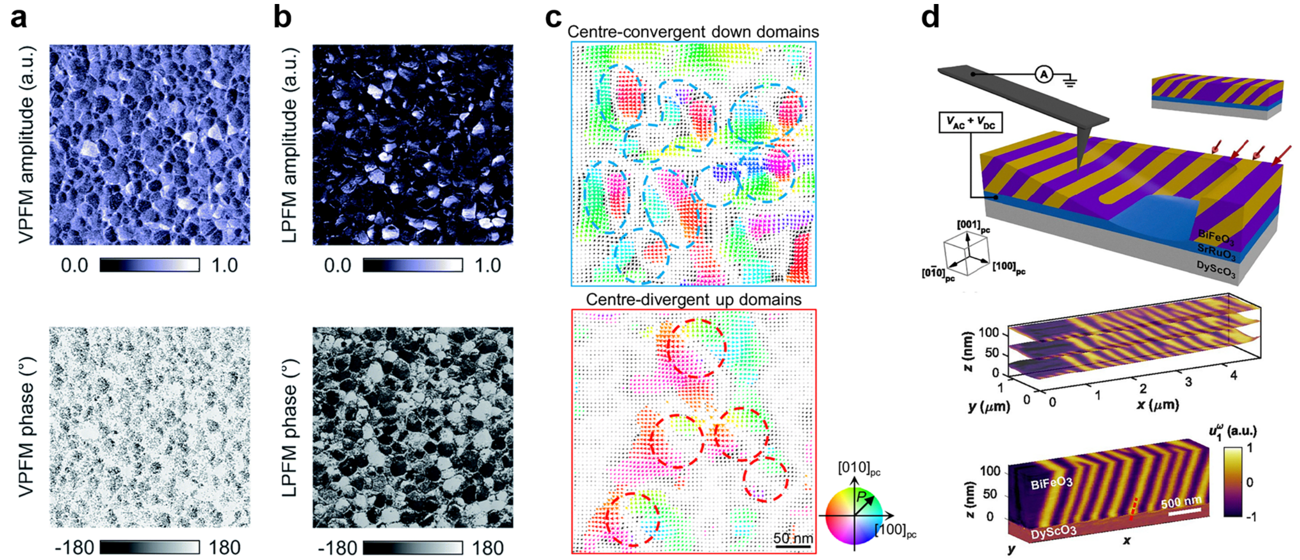

Fig. 3 Advanced PFM techniques for 2D vector mapping and 3D volumetric analysis. (a) VPFM amplitude and phase images, which visualize the P_z by measuring vertical surface displacement. Reproduced with permission.[54] Copyright, 2021 Royal Society of Chemistry. (b) LPFM amplitude and phase images of the same area, mapping the P_x and P_y by detecting the torsional motion of the cantilever. Reproduced with permission.[54] Copyright, 2021 Royal Society of Chemistry. (c) A vector PFM reconstruction of a complex topological domain structure. The vector maps are generated by combining the VPFM and LPFM signals to reveal the complete 2D polarization vector field. Reproduced with permission.[58] Copyright, 2025 Springer Nature. (d) Schematic illustration and resulting 3D domain morphologies for TPFM. Stacking these cross-sectional images generates a full 3D volumetric reconstruction of the internal domain architecture. Reproduced with permission.[60] Copyright, 2018 United States National Academy of Sciences.

screening layer. Furthermore, KPFM can capture dynamic screening effects.[31,48,65] This arises because the screening charge relaxes more slowly than the underlying polarization, providing a direct spatial probe of the screening kinetics (Fig. 4a).[66]

Importantly, the CPD contrast is not solely dependent on the intrinsic polarization but is also highly sensitive to the local environment and surface chemistry. Correlative studies demonstrate that factors such as humidity and photoexcitation can significantly modulate the surface adsorbate population.[63,64] This, in turn, can cause lateral broadening of the measured domain potentials and introduce slow, time-dependent relaxation components, reflecting complex electrochemical processes rather than simple electrostatic discharge (Fig. 4b).[64] Recent advances, such as high-speed sparse-scanning KPFM, further enhance the spatiotemporal capability, enabling the capture of

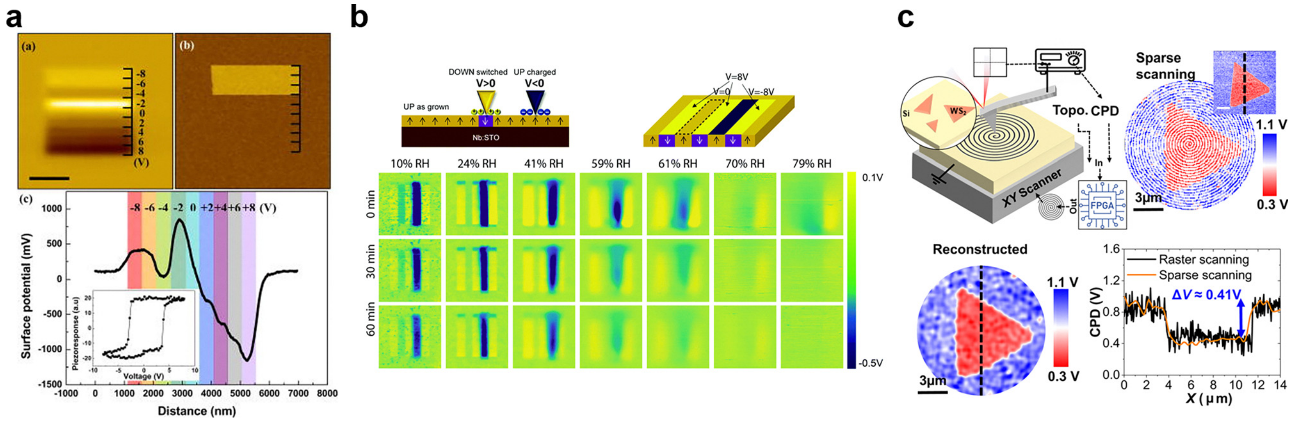

Fig. 4 KPFM analysis of surface electrostatics, screening dynamics, and environmental effects. (a) The local surface potential measured by KPFM and the polarization orientation measured by the PFM phase as a function of an applied DC voltage sweep, demonstrating the relationship between polarization switching and the surface electrostatic state. Reprinted with the permission.[66] Copyright, 2009 AIP Publishing. (b) KPFM images demonstrating the influence of the local environment and surface chemistry. Factors such as humidity can modulate surface adsorbates, leading to slow, time-dependent potential relaxation components reflecting electrochemical processes. Used with permission from the Royal Society of Chemistry,[64] from permission conveyed through Copyright Clearance Center, Inc. Copyright 2019 Royal Society of Chemistry. (c) Illustration and experimental result of high-speed sparse-scanning KPFM, an advanced technique capable of capturing dynamic processes. Reproduced with permission.[67] Copyright, 2023 Springer Nature.

mobile charge dynamics and domain-wall–coupled potentials over large areas, thus linking mesoscale transport phenomena to the underlying nanoscale polarization patterns (Fig. 4c).[67]

C-AFM utilizes a biased tip in contact mode to generate nanoscale current maps. The C-AFM current maps highlight ferroelectric domain walls as distinct conduction pathways relative to the insulating surrounding domains.[68–71] A seminal C-AFM study, for instance, established the existence of room-temperature electronic conduction confined to specific domain walls (Fig. 5a).[32] This behavior was attributed to structurally driven electrostatic potential steps and an accompanying local modification of the electronic band structure, positioning C-AFM as a definitive characterization method for the ferroelectric domain wall-specific transport. The ferroelectric domain wall conductivity is known to depend sensitively on the charge state of the wall such as head-to-head or tail-to-tail geometry.[72] C-AFM can therefore reveal precisely where local band alignment and defect segregation favor carrier injection and subsequent lateral transport along the wall (Fig. 5b).[73] Beyond simply mapping conductivity variations, local current–voltage (I–V) spectroscopy can be performed by positioning the tip precisely on a domain wall (Fig. 5c).[73] This provides a detailed investigation into the specific mechanisms governing charge transport at these nanoscale features, allowing differentiation between Ohmic, Schottky-like, or other conduction behaviors.[74]

Beyond the conventional modalities, novel techniques are emerging to provide deeper insights, particularly into dynamic processes. One such technique is charge gradient microscopy (CGM), which directly interprets how screening charges move and reorganize at ferroelectric surfaces.[75,76] In CGM, a grounded conductive tip scans under a constant applied load. The measured current signal arises from two coupled contributions: (i) a displacement current generated as the tip crosses the spatial gradient of the bound polarization charge at a domain wall (Fig. 6a), and (ii) a triboelectric current associated with the mechanical relocation or scraping of the mobile external screening charges on the domains (Fig. 6b). The magnitude of the CGM current signal scales with the scan velocity, a feature that enables high-speed imaging of domains and walls.[77] Crucially, CGM can also be used to quantify and manipulate the screening state itself. The applied tip load sets a mechanical threshold for removing the external charges, and the subsequent rescreening kinetics can then be monitored. This yields a powerful readout of surface-charge relaxation dynamics, effectively probing the screening environment without altering the underlying bulk polarization (Fig. 6c).[75]

Contact-resonance AFM (CR-AFM) provides a method to probe domain polarity without applying an electrical bias. It relies on electromechanical coupling produced by large, tip-induced strain gradients (Fig. 7a).[78] A sharp tip imposes a highly localized, inhomogeneous deformation, which induces a flexoelectricity – the generation of polarization in dielectric materials under inhomogeneous deformation.[79,80] The flexoelectric contribution superposes with the intrinsic piezoelectric response of the ferroelectric material. The superposition of the polarizations breaks the inversion symmetry of the total mechanical response; consequently, oppositely polarized domains exhibit a measurably different contact stiffness. In CR-AFM, the stiffness difference is detected as a distinct shift in

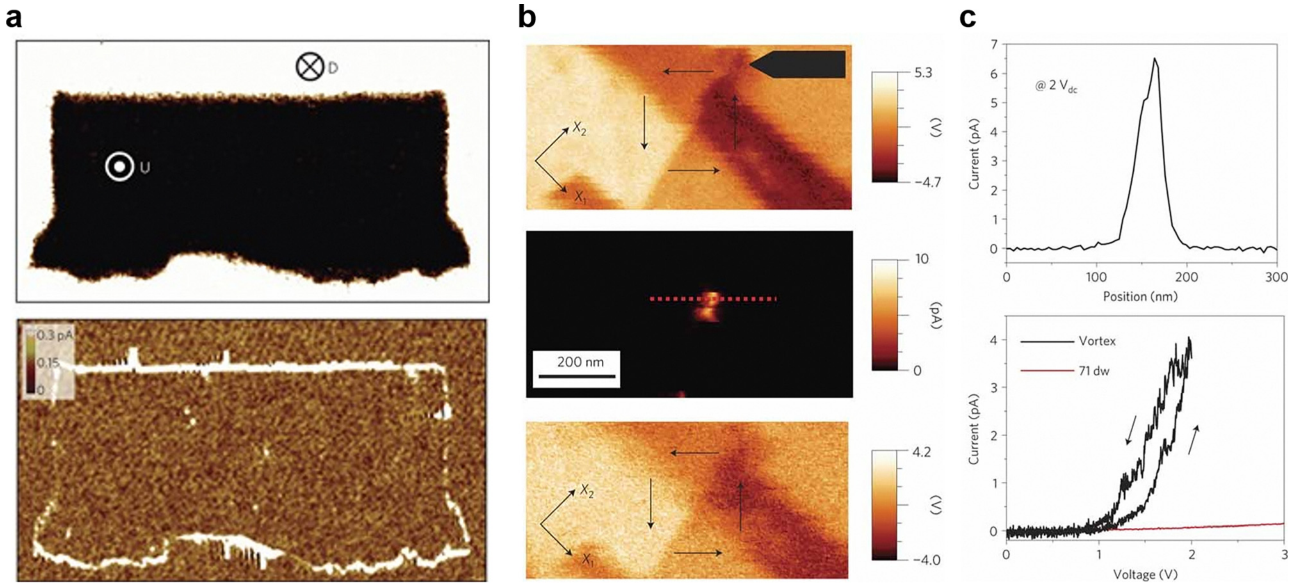

Fig. 5 C-AFM analysis of local electronic transport. (a) PFM phase and corresponding C-AFM current maps establishing electronic conduction confined to a specific 180° domain wall, while the surrounding domains remain insulating. Reproduced with permission.[32] Copyright, 2009 Springer Nature. (b) C-AFM maps revealing how factors such as local band alignment and defect segregation, which are sensitive to the charge state of the domain wall, create favorable conditions for carrier injection and lateral transport. Reproduced with permission.[73] Copyright, 2011 Springer Nature. (c) An example of local I–V spectroscopy, where the C-AFM tip is held stationary on a domain wall to probe the specific mechanisms. Reproduced with permission.[73] Copyright, 2011 Springer Nature.

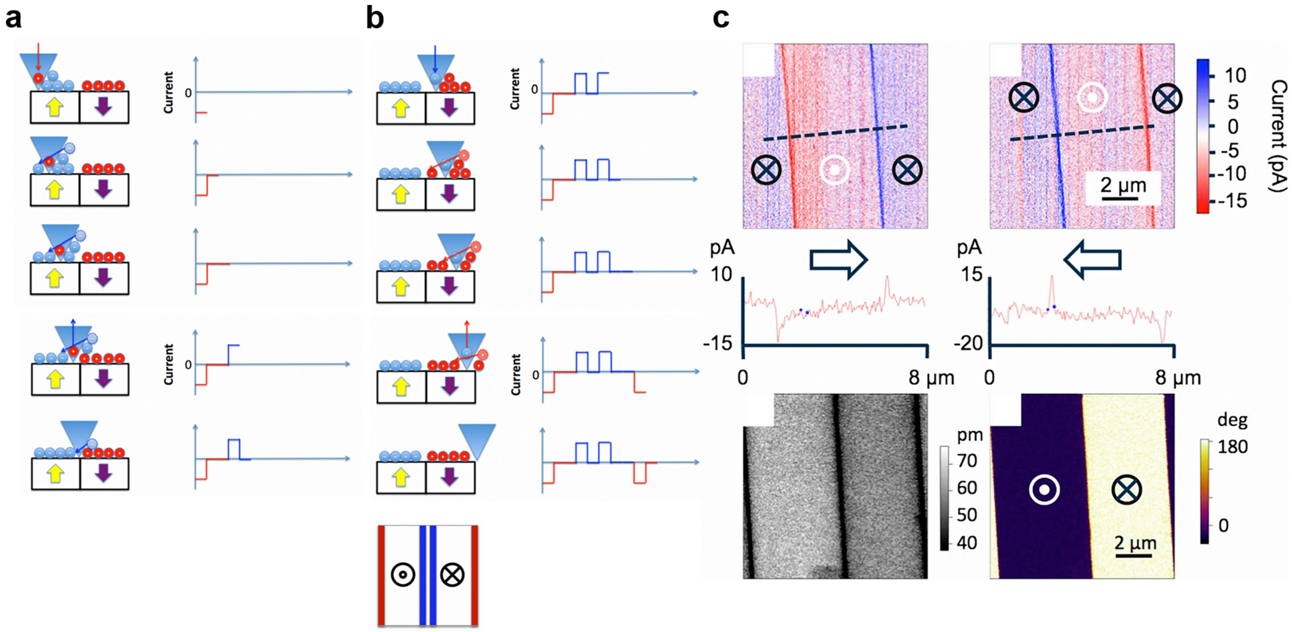

Fig. 6 Probing screening charge dynamics using CGM. (a) and (b) Schematic of the CGM operating principle, which directly images how screening charges move and reorganize on a ferroelectric surface. A grounded tip scanning under constant load measures current from two coupled sources: (a) displacement current at domain walls and (b) triboelectric current from mechanically scraping mobile external screening charges. Reproduced with permission.[71] Copyright, 2013 United States National Academy of Sciences. (c) CGM current maps compared directly with correlative PFM amplitude and phase maps of the same area. Reproduced with permission.[75] Copyright, 2013 United States National Academy of Sciences.

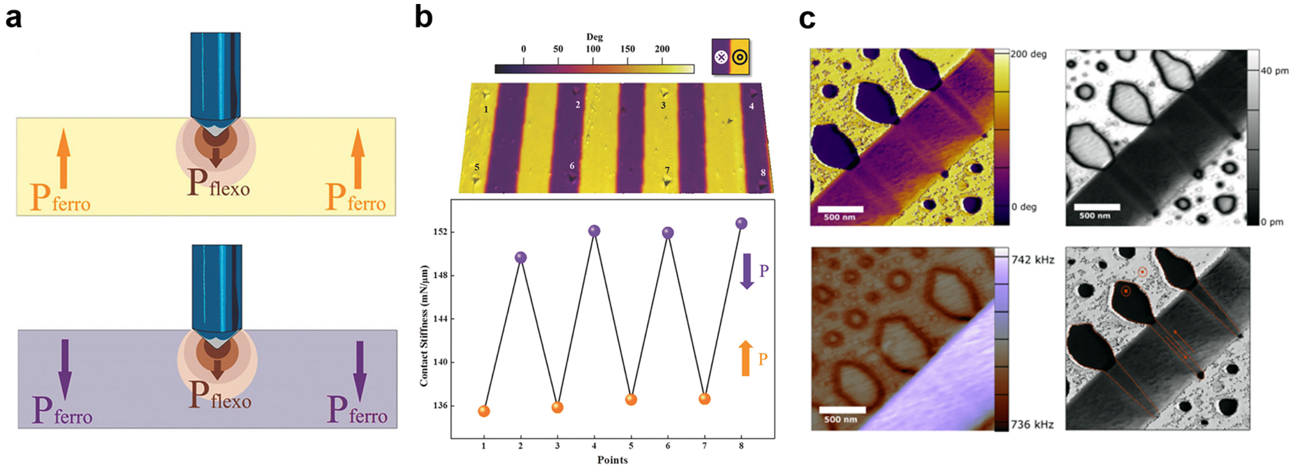

Fig. 7 Probing mechanical properties of domains and walls using CR-AFM. (a) Schematic illustration of the CR-AFM principle, where a sharp tip imposes a large, localized strain gradient to exploit the local electromechanical coupling. Reproduced with permission.[78] Copyright, 2017 Wiley-VCH. (b) CR-AFM resonance frequency variations demonstrating domain polarity mapping. The superposition of the tip-induced flexoelectric response and the intrinsic piezoelectricity of the sample results in a measurable difference in contact stiffness for anti-parallel domains. Reproduced with permission.[78] Copyright, 2017 Wiley-VCH. (c) CR-AFM maps revealing that 180° domain walls are mechanically softer than the surrounding bulk domains, which is attributed to local wall sliding or other electromechanical effects. Reproduced with permission.[82] Copyright, 2017 American Physical Society.

the contact resonance frequency of the cantilever, enabling direct polarity mapping (Fig. 7b).[78] The resonance contrast mechanism, which also allows for quantitative estimates of flexoelectric coupling, naturally strengthens as dimensions shrink and can be optimized using stiffer cantilevers, offering a practical route to a non-destructive, electrode-free readout.[81]

Complementarily, domain walls themselves often furnish a distinct mechanical signature in CR-AFM. 180° domain walls, for instance, are observed to be mechanically softer than the surrounding domains (Fig. 7c).[82] This localized softening is attributed to the tip-induced strain coupling to local domain wall sliding or other depolarization-mediated electromechanical effects, thus provides an additional, domain-wall-specific, and voltage-free contrast channel.

4. Tip-driven manipulation of ferroelectric materials

As mentioned in the earlier section, AFM serves as a powerful platform for the active nanoscale control of ferroelectric materials beyond characterization, enabling manipulation *via* both localized electrical biasing and mechanical stress.[27,83,84] This section will first focus on electrical manipulation, commonly referred to as tip-based poling. In this modality, a conductive AFM tip functions as a highly localized, mobile top electrode. By applying a DC or pulsed voltage that generates a local electric field exceeding the E_C of the ferroelectric material, domains can be written or erased with nanometer precision (Fig. 8a).[85] The switching capability was established in early AFM domain-writing studies and has been widely utilized since.[29,86] The switching process itself is dynamic: as the applied field just surpasses the threshold, switching initiates at energetically favorable nucleation sites. This is followed by the propagation of newly formed domain walls that sweep across the biased region, eventually aligning the entire area. The sequence of the local phase evolution directly reflects the classical understanding of bulk ferroelectric switching, which is interpreted as a process governed by nucleation and subsequent domain growth.[53,87]

Time-resolved studies have further revealed that tip biases can trigger distinct switching pathways – ranging from abrupt 180° reversal to multi-step, ferroelastic-assisted routes – depending on crystallographic orientation and local constraint.[87] PFM has been used to directly visualize intermediate ferroelastic steps during field-driven reversal, linking the

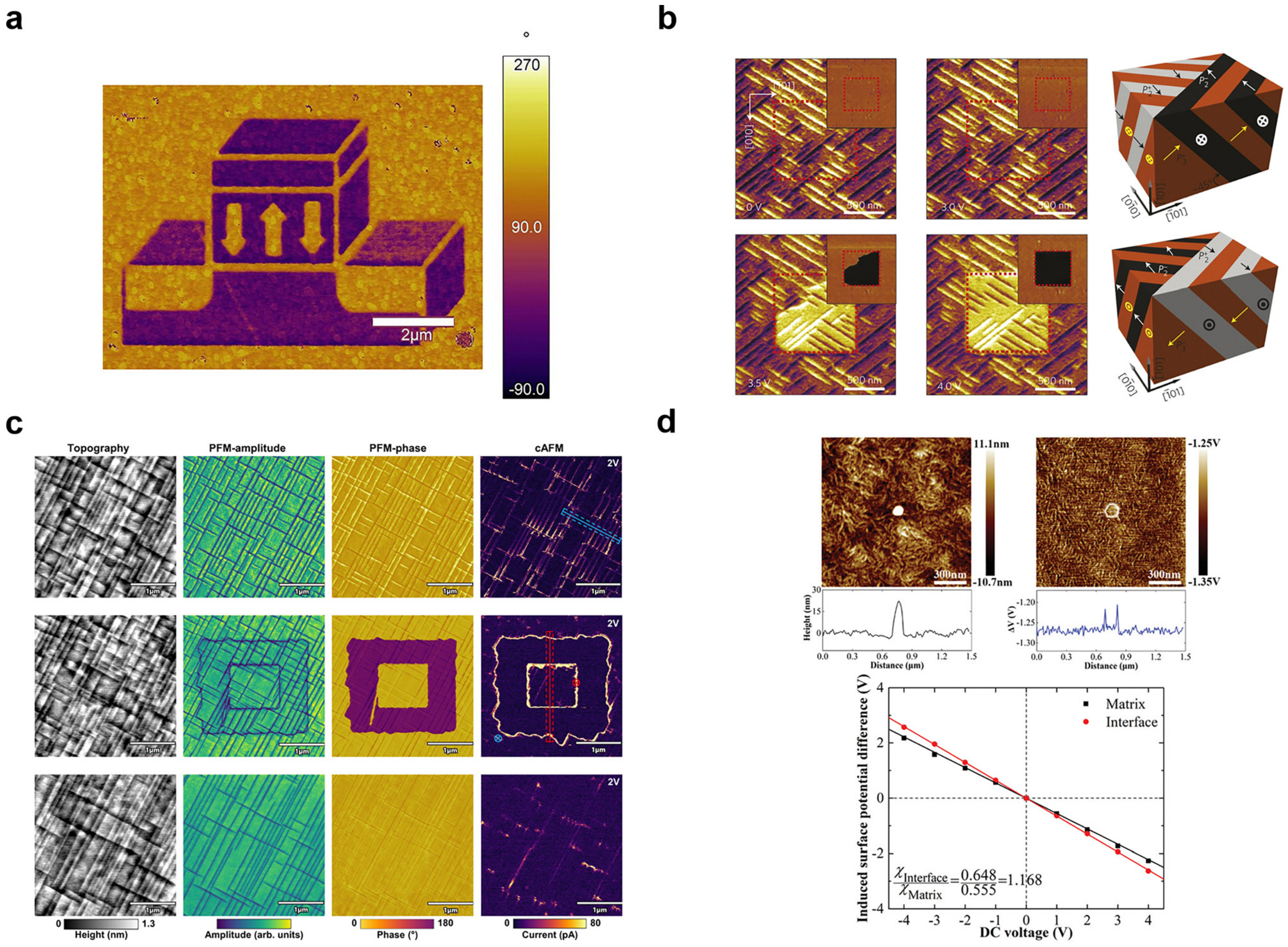

Fig. 8 Nanoscale manipulation of ferroelectric domains and properties using tip-induced electrical stimuli. (a) An example of tip-based electrical poling, where a PFM phase image shows a domain written with nanometer precision by applying a DC voltage from the AFM tip. Reproduced with permission.[85] Copyright, 2024 American Chemical Society. (b) PFM visualization of the switching pathway, visualizing intermediate ferroelastic steps that occur during the polarization reversal process. Reproduced with permission.[88] Copyright, 2014 Springer Nature. (c) Correlative C-AFM data demonstrating that a locally written domain wall acts as an electrically addressable conduction path, governed by the specific charge state and structure of the domain wall. Reproduced with permission.[90] Copyright, 2018 Springer Nature. (d) KPFM measurements on a ferroelectric polymer nanocomposite, revealing enhanced interfacial susceptibility at the organic/inorganic boundary, which influences local switching thresholds and dynamics. Reproduced with permission.[91] Copyright, 2019 Wiley-VCH.

selected pathway to the domain topology and offering routes to accelerate or slow the switching process (Fig. 8b).[88] The tip-based poling also serves as a platform for investigating domain walls themselves. Correlative PFM and C-AFM measurements demonstrate that these locally written or reconfigured domain walls can act as electrically addressable conduction paths.[89,90] The electric transport is governed by the specific charge state and local structure of the domain wall itself, not by the properties of the adjoining domains, thereby recasting domain walls from passive interfaces into active functional entities with distinct, controllable properties (Fig. 8c).[90] Furthermore, electrical manipulation is not confined to ceramic materials. In ferroelectric polymer nanocomposites, the interfacial region between the organic matrix and the embedded inorganic nanomaterial often governs the macroscopic polarization. By combining controlled DC bias with KPFM, researchers have directly detected enhanced interfacial polarization at these organic/inorganic interfaces and interpreted its evolution with local chemistry.[91,92] This finding provides evidence that interfacial dipole ordering and polymer chain mobility, modulated by the surface states of the inorganic fillers, directly influence local switching thresholds and relaxation dynamics (Fig. 8d).[91]

Mechanical manipulation of spontaneous polarization relies mostly on flexoelectricity. As mentioned in the previous section, an AFM tip is uniquely suited to exploit the flexoelectric effect, as it concentrates mechanical stress over a few-nanometer contact region, thereby producing an immense and highly localized strain gradient.[83] The strain gradient, in turn, generates a powerful flexoelectric field capable of biasing or even reversing the local polarization under a sufficiently high applied load (Fig. 9a).[93] This principle is universal and becomes especially potent at the nanoscale where such gradients are maximized.[94,95] Both continuum theory and experiments confirm that normal and frictional loads from a tip generate complex, spatially structured flexoelectric fields that can be used to select specific switching pathways.[96,97] In practice, tip-induced mechanical loading has been used to write and erase domains in oxide films, with the resulting patterns being stable yet also electrically erasable.[93] Beyond static point loading, the trailing strain gradients generated by a moving tip offer an

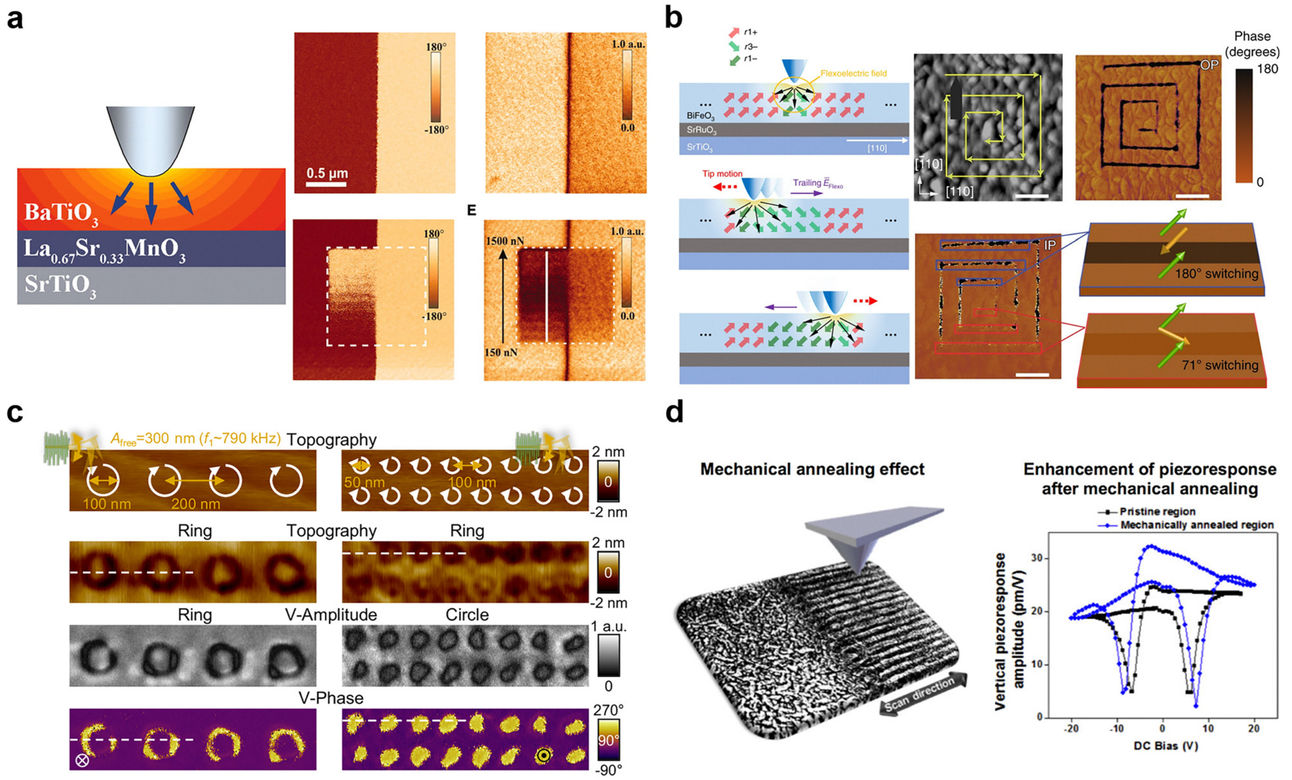

Fig. 9 Nanoscale manipulation of polarization using tip-induced mechanical stress. (a) Schematic illustration and corresponding PFM data demonstrating flexoelectric switching. A high load concentrated at the AFM tip generates a local strain gradient, which produces a flexoelectric field strong enough to reverse the polarization. Reproduced from H. Lu *et al.*, Mechanical Writing of Ferroelectric Polarization, 10.1126/science.1218693 [2012], AAAS.[93] Copyright, 2012 American Association for the Advancement of Science. (b) Illustration and PFM results showing domain writing *via* a scanning tip. The mechanical stress from a scanning tip can be used to steer multi-step switching pathways. Reproduced with permission from Springer Nature.[98] Copyright, 2018 Springer Nature. (c) PFM data showing domain creation using dynamic tapping-mode mechanics. Reproduced with permission.[58] Copyright, 2025 Springer Nature. (d) Schematic and corresponding VPFM spectroscopy results of mechanical annealing in a ferroelectric polymer. The tip-induced stress locally reorients polymer chains to form ordered, polar-phase lamellae with a stronger piezoresponse. Reproduced with permission.[100] Copyright, 2015 American Chemical Society.

additional handle to steer multi-step switching pathways, thus enabling the tuning of switching kinetics without complex voltage waveforms (Fig. 9b).[98]

Recent studies demonstrate that tapping-mode mechanics can extend manipulation beyond continuous contact-mode stress (Fig. 9c).[58] By delivering short, periodic, high-amplitude impulses, an oscillating tip can induce localized phase-boundary softening and generate giant dynamic strain gradients. This has been shown to enable bidirectional mechanical switching and even the creation of exotic skyrmion-like polar nanodomains with long retention times. This single-pass process can simultaneously write polarization domains and sculpt fine topographic features, positioning dynamic tapping as a voltage-free, damage-minimized alternative to contact-mode lithography or milling. Notably, mechanical manipulation is not limited to brittle ceramic materials. In ferroelectric polymers, scanning with a loaded tip can act as a highly localized mechanical annealing process.[99,100] The tip-induced stress causes polymer chain segments to reorient and the microstructure to evolve, forming ordered, polar-phase lamellae. This results in a stronger and more directionally coherent piezoresponse, which is directly observable in co-registered VPFM and LPFM maps (Fig. 9d).[100] This effect is spatially programmable and, importantly, requires neither electrodes nor bulk high-temperature processing.

AFM-based manipulation has become a decisive tool for establishing ferroelectricity in materials where conventional macroscopic hysteresis measurements or device gating are impractical. In 2D layered materials, the distinctions between piezoelectric, ferroelectric, and flexoelectric behaviors become particularly intricate compared to bulk systems.[101] Symmetry breaking in odd-layer configurations can induce piezoelectricity in otherwise non-polar bulk crystals, while sliding ferroelectricity arises from the coupled interlayer shear and out-of-plane polarization.[102,103] Consequently, distinguishing genuine polar switching from extrinsic artifacts requires a spatially resolved approach. Its unique strength lies in the ability to both locally write polarization and immediately read the resulting electromechanical and electrostatic signatures within the same field of view.

For instance, in molybdenum disulfide (MoS_2) – a kind of 2D transition metal dichalcogenides, a mechanical manipulation strategy provided the first room-temperature demonstration of stable domains written purely by tip pressure. Subsequent *in situ* PFM confirmed the polarization reversal, while KPFM mapped the concomitant change in surface potential. This multimodal AFM analysis provided definitive evidence that the flexoelectrically written state was intrinsic and switchable, effectively ruling out charge injection artifacts (Fig. 10a).[104] This mechanical writing concept has been further advanced in other 2D materials, such as copper indium hexathiohypodiphosphate ($CuInP_2S_6$), where the bidirectional flexoelectric domain writing was exploited to demonstrate the reversible polarization switching.[105] Further studies combined advanced interferometric-displacement PFM with KPFM to unambiguously determine the polarization direction and piezoelectric sign after mechanical writing. This illustrates how the combination of AFM manipulation and high-precision metrology can resolve ambiguities that plague purely electrical tests, especially in conductive 2D materials (Fig. 10b).[106]

Furthermore, the electrical-poling approach is crucial for state-of-the-art materials, such as those in complementary metal-oxide-semiconductor (CMOS) technology. In ultra-thin hafnium zirconium oxide ($Hf_xZr_{(1-x)}O_2$) layers, tip-based electrical poling and sequential PFM and KPFM characterization were used to establish inversion-symmetry breaking and robust, rewritable switching.[107–109] This was achieved at thicknesses where conventional electrical characterization fails, and rigorous control experiments successfully ruled out electrostatic artifacts (Fig. 10c).[110] The nanoscale validation using the electrical poling is also vital for wurtzite ferroelectrics, such as aluminium scandium nitride ($Al_{(1-x)}Sc_xN$). In this system, PFM imaging following pulsed voltage application has been used to directly visualize the domain dynamics, revealing the transition from nucleation-limited switching to more uniform reversal and thus confirming the microscopic mechanisms of polarization switching inferred from macroscopic tests (Fig. 10d).[111] More broadly, even when ferroelectricity is inferred from macroscopic device gating in other emergent systems, AFM manipulation provides the indispensable, correlative, and spatially resolved proof of domain formation, stability, and local screening.[105,110–113] It is this capability that fundamentally links nanoscale structure to function, thereby elevating AFM manipulation to a primary validation method for new ferroelectric materials.

5. Perspective and outlook

The application of AFM to ferroelectric materials has fundamentally evolved from a technique for surface topography imaging into an indispensable platform for quantitative nanoscale science. This review has comprehensively described how primary AFM-based methods are now fundamental to understanding the critical link between local structure and the emergent macroscopic properties of ferroelectric materials. Furthermore, the role of AFM has expanded beyond passive characterization. The AFM tip, once viewed only as a probe, is now recognized for its active role in manipulating polarization *via* localized electric fields or mechanical stress, enabling the direct engineering of nanoscale domain architectures.

A key insight consolidated from the reviewed literature is that the complex, non-ideal behaviors observed in ferroelectric materials, such as retention loss, fatigue, and imprint, are direct consequences of nanoscale mechanisms that can be directly visualized with AFM. Indeed, the ability of AFM to provide direct spatial evidence of domain wall pinning at defects, localized switching events, and incomplete charge screening provides the mechanistic understanding that macroscopic measurements cannot. Concurrently, the capacity to precisely write and control nanoscale domains *via* the AFM tip is not merely a fabrication tool; it is a fundamental research

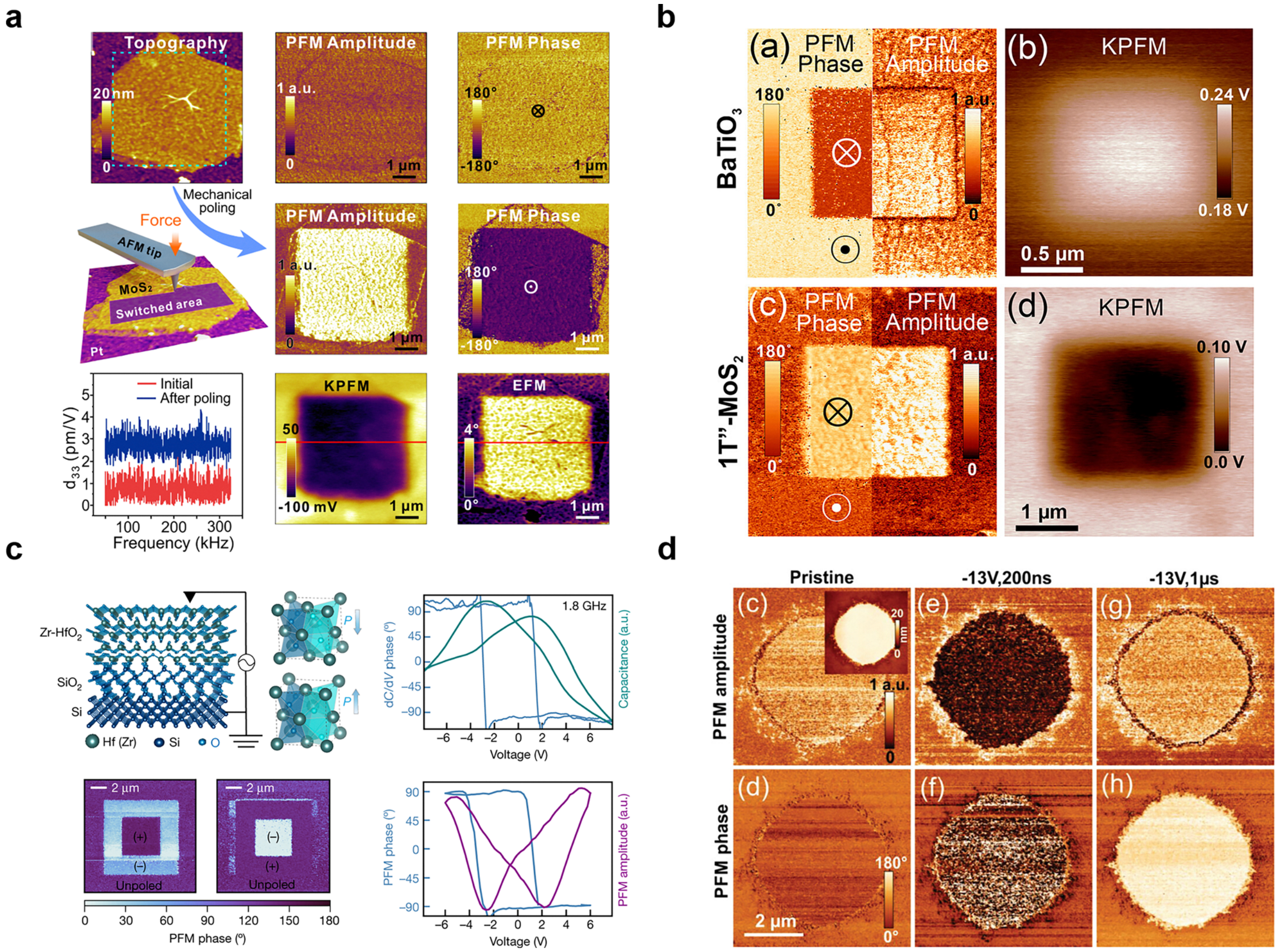

Fig. 10 AFM-based manipulation as a primary validation tool for establishing ferroelectricity in emergent materials. (a) PFM and KPFM images, providing definitive evidence of mechanically induced ferroelectricity in a 2D material, MoS_2. Reproduced with permission.[104] Copyright, 2022 Springer Nature. (b) Use of high-precision metrology, such as interferometric-displacement PFM combined with KPFM, to unambiguously determine the polarization direction and piezoelectric sign after mechanical writing in conductive 2D materials. Reprinted with permission.[106] Copyright, 2023 American Chemical Society. (c) PFM characterization of electrically poled ultra-thin $Hf_xZr_{(1-x)}O_2$, demonstrating rewritable ferroelectric switching in CMOS-compatible layers too thin for conventional electrical characterization. Reproduced with permission.[110] Copyright, 2020 Springer Nature. (d) PFM images of $Al_{(1-x)}Sc_xN$ after pulsed voltage application, directly visualizing the nanoscale domain dynamics and confirming the microscopic switching mechanisms. Reproduced with permission.[111] Copyright, 2024 Wiley-VCH.

method. It enables the creation of precisely defined model systems, such as isolated domains or engineered domain walls, allowing for the systematic study of nanoscale physics that was previously inaccessible.

Despite the remarkable progress, significant challenges must be addressed to elevate the field further. A primary concern is the prevalence of measurement artifacts, particularly nonlocal electrostatic forces between the AFM cantilever body and the sample. These interactions can easily be misinterpreted, creating 'false ferroelectric' hysteresis or errors that distort the measured local electromechanical properties, thereby complicating the validation of emergent ferroelectricity in novel materials.[114,115] Secondly, conventional AFM imaging is inherently slow, which introduces two problems: (i) measurements of small, localized areas may lack statistical representativeness of the bulk material, and (ii) the scan speed is often insufficient to capture the real-time dynamics of fast processes, such as domain wall motion during a sub-microsecond pulse.[116]

Future progress in this field will, therefore, depend on a synergistic advancement in both instrumentation and data analytics. On the hardware front, innovations in high-speed AFM provides the necessary temporal resolution to capture domain dynamics *in situ*, while also enabling the rapid acquisition of large-area maps.[117,118] The high-throughput capability is crucial for acquiring statistically relevant datasets to understand how local heterogeneity governs bulk properties. Concurrently, advanced detectors, such as interferometric displacement sensors (IDSs), are essential for decoupling the true tip-sample response from cantilever-based electrostatic artifacts.[119] An IDS directly measures the true displacement of the tip, and can be focused to be insensitive to the bending modes of the cantilever, enabling truly quantitative and reliable electromechanical measurements.

On the data analytics front, the sheer volume and complexity of data generated by high-speed, multi-modal imaging acquired simultaneously over time render manual analysis intractable. This is where machine learning (ML) and deep learning (DL) are becoming transformative. As demonstrated in recent studies, DL workflows can automatically segment complex domain structures from noisy experimental data.[120–123] More importantly, they can disentangle the underlying physical mechanisms, such as identifying specific domain wall pinning sites from complex time-series images, a task that is nearly impossible for human interpreters.[124] The integration of high-speed, artifact-free hardware with AI-driven analytics represents a definitive shift from static imaging toward dynamic, multidimensional, and statistically meaningful probing. This approach will establish AFM not merely as a characterization tool, but as a key platform for the rational design and controlled nanofabrication in ferroelectric materials research.

Author contributions

Y. K. and K. P. contributed equally to this work. Y.K. and K. P. wrote the original draft. S.Han, D.C., D.K., and G. K. provided constructive comment on the manuscript. S. Hong supervised the project and edited the manuscript.

Conflicts of interest

The authors declare no competing interests

Data availability

No primary research results, software or code have been included and no new data were generated or analyzed as part of this review.

Acknowledgements

This work was supported by the National Research Foundation of Korea (NRF) grant funded by the Korea government (MSIT) (RS-2023-00247245).

References

1 J. Valasek, *Phys. Rev.*, 1921, **17**, 475.
2 D. Damjanovic, *Rep. Prog. Phys.*, 1998, **61**, 1267–1324.
3 H. Seungbum and SpringerLink, *Nanoscale Phenomena in Ferroelectric Thin Films*, Springer US: Imprint: Springer, New York, NY, 1st edn, 2004.
4 R. E. Cohen, *Nature*, 1992, **358**, 136–138.
5 A. Von Hippel, R. G. Breckenridge, F. G. Chesley and L. Tisza, *Ind. Eng. Chem.*, 1946, **38**, 1097–1109.
6 S. Roberts, *Phys. Rev.*, 1947, **71**, 890.
7 *Nat. Mater.*, 2020, **19**, 129.
8 J. F. Scott, *Science*, 2007, **315**, 954–959.
9 J. F. Scott and C. A. Paz de Araujo, *Science*, 1989, **246**, 1400–1405.
10 R. W. Whatmore, *Rep. Prog. Phys.*, 1986, **49**, 1335–1386.
11 H. Jaffe, *J. Am. Ceram. Soc.*, 1958, **41**, 494–498.
12 Z. L. Wang and J. H. Song, *Science*, 2006, **312**, 242–246.
13 M. E. Lines and A. M. Glass, *Principles and applications of ferroelectrics and related materials*, Clarendon Press, Oxford, 1977.
14 N. Setter, D. Damjanovic, L. Eng, G. Fox, S. Gevorgian, S. Hong, A. Kingon, H. Kohlstedt, N. Y. Park, G. B. Stephenson, I. Stolitchnov, A. K. Taganstev, D. V. Taylor, T. Yamada and S. Streiffer, *J. Appl. Phys.*, 2006, **100**, 051606.
15 D. Damjanovic, *The science of hysteresis*, 2006, vol. 3, 337–465.
16 R. Bulanadi, K. Cordero-Edwards, P. Tueckmantel, S. Saremi, G. Morpurgo, Q. Zhang, L. W. Martin, V. Nagarajan and P. Paruch, *Phys. Rev. Lett.*, 2024, **133**, 106801.
17 W. J. Merz, *Phys. Rev.*, 1954, **95**, 690.
18 M. Dawber, K. M. Rabe and J. F. Scott, *Rev. Mod. Phys.*, 2005, **77**, 1083–1130.
19 M. Hayashi, *J. Phys. Soc. Jpn.*, 1973, **34**, 1686.
20 A. K. Tagantsev, L. E. Cross, J. Fousek and SpringerLink, *Domains in ferroic crystals and thin films*, Springer, New York, 1st edn, 2010.
21 L. Zhang, W. L. Zhong, C. L. Wang, Y. P. Peng and Y. G. Wang, *Eur. Phys. J. B*, 1999, **11**, 565–573.
22 A. Gruverman and A. Kholkin, *Rep. Prog. Phys.*, 2006, **69**, 2443–2474.
23 S. V. Kalinin and D. A. Bonnell, *Phys. Rev. B:Condens. Matter Mater. Phys.*, 2002, **65**, 125408.
24 A. Gruverman, O. Auciello and H. Tokumoto, *Annu. Rev. Mater. Sci.*, 1998, **28**, 101–123.
25 S. V. Kalinin and A. Gruverman, *Scanning probe microscopy: electrical and electromechanical phenomena at the nanoscale*, Springer, New York, 2007.
26 P. Guthner and K. Dransfeld, *Appl. Phys. Lett.*, 1992, **61**, 1137–1139.
27 O. Kolosov, A. Gruverman, J. Hatano, K. Takahashi and H. Tokumoto, *Phys. Rev. Lett.*, 1995, **74**, 4309–4312.
28 E. L. Colla, S. B. Hong, D. V. Taylor, A. K. Tagantsev, N. Setter and K. No, *Appl. Phys. Lett.*, 1998, **72**, 2763–2765.
29 S. Hong, E. L. Colla, E. Kim, D. V. Taylor, A. K. Tagantsev, P. Muralt, K. No and N. Setter, *J. Appl. Phys.*, 1999, **86**, 607–613.
30 S. Hong, J. Woo, H. Shin, J. U. Jeon, Y. E. Pak, E. L. Colla, N. Setter, E. Kim and K. No, *J. Appl. Phys.*, 2001, **89**, 1377–1386.
31 S. V. Kalinin and D. A. Bonnell, *Phys. Rev. B:Condens. Matter Mater. Phys.*, 2001, **63**, 125411.
32 J. Seidel, L. W. Martin, Q. He, Q. Zhan, Y. H. Chu, A. Rother, M. E. Hawkridge, P. Maksymovych, P. Yu, M. Gajek, N. Balke, S. V. Kalinin, S. Gemming, F. Wang, G. Catalan, J. F. Scott, N. A. Spaldin, J. Orenstein and R. Ramesh, *Nat. Mater.*, 2009, **8**, 229–234.

33 A. Gruverman, M. Alexe and D. Meier, *Nat. Commun.*, 2019, **10**, 1661.

34 G. Busch and P. Scherrer, *Naturwissenschaften*, 1935, **23**, 737.

35 F. Bernardini, V. Fiorentini and D. Vanderbilt, *Phys. Rev. B:Condens. Matter Mater. Phys.*, 1997, **56**, 10024–10027.

36 A. Devonshire, *Adv. Phys.*, 1954, **3**, 85–130.

37 A. N. Morozovska, E. A. Eliseev, S. L. Bravina and S. V. Kalinin, *J. Appl. Phys.*, 2011, **110**, 052011.

38 E. A. Little, *Phys. Rev.*, 1955, **98**, 978.

39 R. Landauer, *J. Appl. Phys.*, 1957, **28**, 227–234.

40 R. R. Mehta, B. D. Silverman and J. T. Jacobs, *J. Appl. Phys.*, 1973, **44**, 3379–3385.

41 S. J. Oshea, R. M. Atta, M. P. Murrell and M. E. Welland, *J. Vac. Sci. Technol., B*, 1995, **13**, 1945–1952.

42 M. Nonnenmacher, M. P. Oboyle and H. K. Wickramasinghe, *Appl. Phys. Lett.*, 1991, **58**, 2921–2923.

43 S. Hong, *J. Appl. Phys.*, 2021, **129**, 051101.

44 B. J. Rodriguez, C. Callahan, S. V. Kalinin and R. Proksch, *Nanotechnology*, 2007, **18**, 475504.

45 R. K. Vasudevan, N. Balke, P. Maksymovych, S. Jesse and S. V. Kalinin, *Appl. Phys. Rev.*, 2017, **4**, 021302.

46 A. Gannepalli, D. G. Yablon, A. H. Tsou and R. Proksch, *Nanotechnology*, 2011, **22**, 355705.

47 W. Melitz, J. Shen, A. C. Kummel and S. Lee, *Surf. Sci. Rep.*, 2011, **66**, 1–27.

48 X. Q. Chen, H. Yamada, T. Horiuchi, K. Matsushige, S. Watanabe, M. Kawai and P. S. Weiss, *J. Vac. Sci. Technol., B*, 1999, **17**, 1930–1934.

49 M. Lanza, *Conductive atomic force microscopy: applications in nanomaterials*, Wiley-VCH, Weinheim, Germany, 2017.

50 J. Seidel, P. Maksymovych, Y. Batra, A. Katan, S. Y. Yang, Q. He, A. P. Baddorf, S. V. Kalinin, C. H. Yang, J. C. Yang, Y. H. Chu, E. K. H. Salje, H. Wormeester, M. Salmeron and R. Ramesh, *Phys. Rev. Lett.*, 2010, **105**, 197603.

51 C. H. Yang, J. Seidel, S. Y. Kim, P. B. Rossen, P. Yu, M. Gajek, Y. H. Chu, L. W. Martin, M. B. Holcomb, Q. He, P. Maksymovych, N. Balke, S. V. Kalinin, A. P. Baddorf, S. R. Basu, M. L. Scullin and R. Ramesh, *Nat. Mater.*, 2009, **8**, 485–493.

52 A. Roelofs, U. Böttger, R. Waser, F. Schlaphof, S. Trogisch and L. M. Eng, *Appl. Phys. Lett.*, 2000, **77**, 3444–3446.

53 H. Okino, T. Ida, H. Ebihara, H. Yamada, K. Matsushige and T. Yamamoto, *Jpn. J. Appl. Phys. 1*, 2001, **40**, 5828–5832.

54 T. Leonhard, H. Röhm, F. J. Altermann, M. J. Hoffmann and A. Colsmann, *J. Mater. Chem. A*, 2021, **9**, 21845–21858.

55 M. Checa, B. Pant, A. Puretzky, B. Dryzhakov, R. K. Vasudevan, Y. T. Liu, P. Kavle, A. Dasgupta, L. W. Martin, Y. Cao, L. Collins, S. Jesse, N. Domingo and K. P. Kelley, *Nat. Nanotechnol.*, 2025, **20**, 43–50.

56 M. Park, S. Hong, J. A. Klug, M. J. Bedzyk, O. Auciello, K. No and A. Petford-Long, *Appl. Phys. Lett.*, 2010, **97**, 112907.

57 K. Chu and C. H. Yang, *Rev. Sci. Instrum.*, 2018, **89**, 123704.

58 J. Kim, Y. Yeo, Y. J. Kwon, J. Lee, J. Seo, S. Hong and C. H. Yang, *Npj Quantum Mater.*, 2025, **10**, 71.

59 M. F. Guo, E. X. Xu, H. B. Huang, C. Q. Guo, H. T. Chen, S. L. Chen, S. He, L. Zhou, J. Ma, Z. H. Shen, B. Xu, D. Yi, P. Gao, C. W. Nan, N. D. Mathur and Y. Shen, *Nat. Commun.*, 2024, **15**, 348.

60 J. J. Steffes, R. A. Ristau, R. Ramesh and B. D. Huey, *Proc. Natl. Acad. Sci. U. S. A.*, 2019, **116**, 2413–2418.

61 Y. Tikhonov, J. R. Maguire, C. J. McCluskey, J. P. McConville, A. Kumar, H. D. Lu, D. Meier, A. Razumnaya, J. M. Gregg, A. Gruverman, V. M. Vinokur and I. Luk'yanchuk, *Adv. Mater.*, 2022, **34**, 2203028.

62 E. Gradauskaite, Q. N. Meier, N. Gray, M. F. Sarott, T. Scharsach, M. Campanini, T. Moran, A. Vogel, K. Del Cid-Ledezma, B. D. Huey, M. D. Rossell, M. Fiebig and M. Trassin, *Nat. Mater.*, 2023, **22**, 1492–1498.

63 I. Gaponenko, L. Musy, N. Domingo, N. Stucki, A. Verdaguer, N. Bassiri-Gharb and P. Paruch, *Npj Comput. Mater.*, 2021, **7**, 163.

64 N. Domingo, I. Gaponenko, K. Cordero-Edwards, N. Stucki, V. Pérez-Dieste, C. Escudero, E. Pach, A. Verdaguer and P. Paruch, *Nanoscale*, 2019, **11**, 17920–17930.

65 S. V. Kalinin and D. A. Bonnell, *Nano Lett.*, 2004, **4**, 555–560.

66 Y. Kim, C. Bae, K. Ryu, H. Ko, Y. K. Kim, S. Hong and H. Shin, *Appl. Phys. Lett.*, 2009, **94**, 032907.

67 M. Checa, A. S. Fuhr, C. H. Y. Sun, R. Vasudevan, M. Ziatdinov, I. Ivanov, S. J. Yun, K. Xiao, A. Sehirlioglu, Y. Kim, P. Sharma, K. P. Kelley, N. Domingo, S. Jesse and L. Collins, *Nat. Commun.*, 2023, **14**, 7196.

68 J. Schultheiss, E. Lysne, L. Puntigam, J. Schaab, E. Bourret, Z. W. Yan, S. Krohns and D. Meier, *Nano Lett.*, 2021, **21**, 9560–9566.

69 A. Suna, O. E. Baxter, J. P. V. McConville, A. Kumar, R. G. P. McQuaid and J. M. Gregg, *Appl. Phys. Lett.*, 2022, **121**, 222902.

70 H. W. Shin and J. Y. Son, *Ceram. Int.*, 2023, **49**, 2786–2791.

71 L. Richarz, I. C. Skogvoll, E. Y. Tokle, K. A. Hunnestad, U. Ludacka, J. L. He, E. Bourret, Z. W. Yan, A. T. J. van Helvoort, J. Schultheiss, S. M. Selbach and D. Meier, *ACS Appl. Mater. Interfaces*, 2025, **17**, 47576–47584.

72 X. F. Wu and D. Vanderbilt, *Phys. Rev. B:Condens. Matter Mater. Phys.*, 2006, **73**, 020103.

73 N. Balke, B. Winchester, W. Ren, Y. H. Chu, A. N. Morozovska, E. A. Eliseev, M. Huijben, R. K. Vasudevan, P. Maksymovych, J. Britson, S. Jesse, I. Kornev, R. Ramesh, L. Bellaiche, L. Q. Chen and S. V. Kalinin, *Nat. Phys.*, 2012, **8**, 81–88.

74 J. Jiang, Z. L. Bai, Z. H. Chen, L. He, D. W. Zhang, Q. H. Zhang, J. A. Shi, M. H. Park, J. F. Scott, C. S. Hwang and A. Q. Jiang, *Nat. Mater.*, 2018, **17**, 49–56.

75 S. Hong, S. Tong, W. I. Park, Y. Hiranaga, Y. S. Cho and A. Roelofs, *Proc. Natl. Acad. Sci. U. S. A.*, 2014, **111**, 6566–6569.

76 S. Tong, W. I. Park, Y. Y. Choi, L. Stan, S. Hong and A. Roelofs, *Phys. Rev. Appl.*, 2015, **3**, 014003.

77 S. Tong, I. W. Jung, Y. Y. Choi, S. Hong and A. Roelofs, *ACS Nano*, 2016, **10**, 2568–2574.

78 K. Cordero-Edwards, N. Domingo, A. Abdollahi, J. Sort and G. Catalan, *Adv. Mater.*, 2017, 29.

79 T. D. Nguyen, S. Mao, Y. W. Yeh, P. K. Purohit and M. C. McAlpine, *Adv. Mater.*, 2013, **25**, 946–974.

80 P. Zubko, G. Catalan and A. K. Tagantsev, *Annu. Rev. Mater. Res.*, 2013, **43**, 387–421.

81 C. Stefani, E. Langenberg, K. Cordero-Edwards, D. G. Schlom, G. Catalan and N. Domingo, *J. Appl. Phys.*, 2021, **130**, 074103.

82 C. Stefani, L. Ponet, K. Shapovalov, P. Chen, E. Langenberg, D. G. Schlom, S. Artyukhin, M. Stengel, N. Domingo and G. Catalan, *Phys. Rev. X*, 2020, **10**, 041001.

83 A. L. Kholkin, V. V. Shvartsman, A. Y. Emelyanov, R. Poyato, M. L. Calzada and L. Pardo, *Appl. Phys. Lett.*, 2003, **82**, 2127–2129.

84 S. Jesse, A. P. Baddorf and S. V. Kalinin, *Appl. Phys. Lett.*, 2006, **88**, 062908.

85 S. Yun, H. Kim, M. Seo, M. H. Kang, T. Kim, S. Cho, M. H. Park, S. Jeon, Y. K. Choi and S. Hong, *ACS Appl. Electron. Mater.*, 2024, **6**, 2134–2141.

86 T. Tybell, P. Paruch, T. Giamarchi and J. M. Triscone, *Phys. Rev. Lett.*, 2002, **89**, 097601.

87 P. Tückmantel, I. Gaponenko, N. Caballero, J. C. Agar, L. W. Martin, T. Giamarchi and P. Paruch, *Phys. Rev. Lett.*, 2021, **126**, 117601.

88 R. J. Xu, S. Liu, I. Grinberg, J. Karthik, A. R. Damodaran, A. M. Rappe and L. W. Martin, *Nat. Mater.*, 2015, **14**, 79–86.

89 P. Sharma, Q. Zhang, D. Sando, C. H. Lei, Y. Y. Liu, J. Y. Li, V. Nagarajan and J. Seidel, *Sci. Adv.*, 2017, **3**, e1700512.

90 F. Risch, Y. Tikhonov, I. Lukyanchuk, A. M. Ionescu and I. Stolichnov, *Nat. Commun.*, 2022, **13**, 7239.

91 S. M. Peng, X. Yang, Y. Yang, S. J. Wang, Y. Zhou, J. Hu, Q. Li and J. L. He, *Adv. Mater.*, 2019, **31**, 1807722.

92 Y. G. Kim, K. T. Kim, S. C. Park, D. H. Heo, D. Y. Hyeon, S. P. R. Mallem and K. I. Park, *Nano Energy*, 2022, 98.

93 H. Lu, C. W. Bark, D. E. de los Ojos, J. Alcala, C. B. Eom, G. Catalan and A. Gruverman, *Science*, 2012, **336**, 59–61.

94 G. Catalan, L. J. Sinnamon and J. M. Gregg, *J. Phys. Condens. Mater.*, 2004, **16**, 2253–2264.

95 D. Lee, A. Yoon, S. Y. Jang, J. G. Yoon, J. S. Chung, M. Kim, J. F. Scott and T. W. Noh, *Phys. Rev. Lett.*, 2011, **107**, 057602.

96 J. Ocenásek, H. Lu, C. W. Bark, C. B. Eom, J. Alcalá, G. Catalan and A. Gruverman, *Phys. Rev. B:Condens. Matter Mater. Phys.*, 2015, **92**, 035417.

97 S. Das, B. Wang, T. R. Paudel, S. M. Park, E. Y. Tsymbal, L. Q. Chen, D. Lee and T. W. Noh, *Nat. Commun.*, 2019, **10**, 537.

98 S. M. Park, B. Wang, S. Das, S. C. Chae, J. S. Chung, J. G. Yoon, L. Q. Chen, S. M. Yang and T. W. Noh, *Nat. Nanotechnol.*, 2018, **13**, 366–370.

99 R. Roth, M. M. Koch, A. D. Rata and K. Dörr, *Adv. Electron. Mater.*, 2022, **8**, 2101416.

100 Y. Y. Choi, P. Sharma, C. Phatak, D. J. Gosztola, Y. Y. Liu, J. Lee, B. Lee, J. Y. Li, A. Gruverman, S. Ducharme and S. Hong, *ACS Nano*, 2015, **9**, 1809–1819.

101 W. B. Li, X. F. Qian and J. Li, *Nat. Rev. Mater.*, 2021, **6**, 829–846.

102 L. Li and M. H. Wu, *ACS Nano*, 2017, **11**, 6382–6388.

103 M. H. Wu and J. Li, *Proc. Natl. Acad. Sci. U. S. A.*, 2022, **118**, e2115703118.

104 A. Lipatov, P. Chaudhary, Z. Guan, H. D. Lu, G. Li, O. Crégut, K. D. Dorkenoo, R. Proksch, S. Cherifi-Hertel, D. F. Shao, E. Y. Tsymbal, J. Iñiguez, A. Sinitskii and A. Gruverman, *Npj 2D Mater. Appl.*, 2022, **6**, 18.

105 H. Liu, Q. L. Lai, J. Fu, S. J. Zhang, Z. M. Fu and H. L. Zeng, *Nat. Commun.*, 2024, **15**, 4556.

106 H. D. Lu, H. Aramberri, A. Lipatov, R. Proksch, A. Sinitskii, J. Iñiguez and A. Gruverman, *ACS Mater. Lett.*, 2023, **5**, 3136–3141.

107 H. D. Lu, D. J. Kim, H. Aramberri, M. Holzer, P. Buragohain, S. Dutta, U. Schroeder, V. Deshpande, J. Iniguez, A. Gruverman and C. Dubourdieu, *Nat. Commun.*, 2024, **15**, 860.

108 J. Zhu, Y. Y. Wu, H. N. Li, L. Wang, Y. Q. Wang, X. Q. Liu, Y. X. He, S. W. Zhang, J. Su, T. Li, H. H. Ma, J. C. Zhang and Y. Hao, *AIP Adv.*, 2025, **15**, 035350.

109 K. de Hond, M. Salverda, M. Ahmadi, E. Houwman, B. Noheda, B. J. Kooi, G. Rijnders and G. Koster, *ACS Appl. Electron. Mater.*, 2025, **7**, 8013–8019.

110 Y. Yun, P. Buragohain, M. Li, Z. Ahmadi, Y. Z. Zhang, X. Li, H. H. Wang, J. Li, P. Lu, L. L. Tao, H. Y. Wang, J. E. Shield, E. Y. Tsymbal, A. Gruverman and X. S. Xu, *Nat. Mater.*, 2022, **21**, 903–909.

111 H. D. Lu, G. Schönweger, A. Petraru, H. Kohlstedt, S. Fichtner and A. Gruverman, *Adv. Funct. Mater.*, 2024, **34**, 2315169.

112 A. Belianinov, Q. He, A. Dziaugys, P. Maksymovych, E. Eliseev, A. Borisevich, A. Morozovska, J. Banys, Y. Vysochanskii and S. V. Kalinin, *Nano Lett.*, 2015, **15**, 3808–3814.

113 S. Baek, H. H. Yoo, J. H. Ju, P. Sriboriboon, P. Singh, J. J. Niu, J. H. Park, C. Shin, Y. Kim and S. Lee, *Adv. Sci.*, 2022, **9**, 2200566.

114 S. Bradler, A. Schirmeisen and B. Roling, *J. Appl. Phys.*, 2018, **123**, 035106.

115 M. Litterst, A. A. Butkevich and M. Kemerink, *Nature*, 2025, **644**, E1–E3.

116 B. N. Slautin, Y. T. Liu, K. Barakati, Y. Liu, R. Emery, S. Hong, A. Dubey, V. V. Shvartsman, D. C. Lupascu, S. L. Sanchez, M. Ahmadi, Y. Kim, E. Strelcov, K. A. Brown, P. D. Rack and S. V. Kalinin, *Appl. Phys. Rev.*, 2025, **12**, 031321.

117 T. Ando, N. Kodera, E. Takai, D. Maruyama, K. Saito and A. Toda, *Proc. Natl. Acad. Sci. U. S. A.*, 2001, **98**, 12468–12472.

118 T. Ando, *Nanotechnology*, 2012, **23**, 062001.

119 L. Collins, Y. T. Liu, O. S. Ovchinnikova and R. Proksch, *ACS Nano*, 2019, **13**, 8055–8066.

120 Y. T. Liu, M. A. Ziatdinov, R. K. Vasudevan and S. V. Kalinin, *Patterns*, 2023, **4**, 100858.

121 Y. Liu, B. Slautin, J. Bemis, R. Proksch, R. Pant, I. Takeuchi, S. Udovenko, S. Trolier-McKinstry and S. V. Kalinin, *Appl. Phys. Lett.*, 2025, **126**, 042901.

122 Y. Liu, R. Proksch, J. Bemis, U. Pratiush, A. Dubey, M. Ahmadi, R. Emery, P. D. Rack, Y. C. Liu, J. C. Yang and S. V. Kalinin, *ACS Nano*, 2025, **19**, 19659–19669.

123 P. Sriboriboon, H. M. Qiao, O. Kwon, R. K. Vasudevan, S. Jesse and Y. Kim, *Npj Comput. Mater.*, 2023, **9**, 28.

124 K. Barakati, Y. Liu, C. Nelson, M. Ziatdinov, X. Zhang, I. Takeuchi and S. V. Kalinin, *Adv. Mater.*, 2025, **37**, e2418927.